ChemComm

Design and synthesis of aryl-functionalized carbazole-based porous coordination cages

Journal:	*ChemComm*
Manuscript ID	CC-COM-06-2020-003910.R1
Article Type:	Communication

COMMUNICATION

Design and synthesis of aryl-functionalized carbazole-based porous coordination cages

Received 00th January 20xx,
Accepted 00th January 20xx

DOI: 10.1039/x0xx00000x

Casey A. Rowland,[a] Gregory R. Lorzing,[a,b] Rameswar Bhattacharjee,[c] Stavros Caratzoulas,[c] Glenn P. A. Yap[a] and Eric D. Bloch*[a,b,c]

A subset of coordination cages have garnered considerable recent attention for their potential permanent porosity in the solid state. Herein, we report a series of functionalized carbazole-based cages of the structure type M_{12}(R-cdc)$_{12}$ (M = Cr, Cu, Mo) where the functional groups include a range of aromatic substituents. Single-crystal X-ray structure determinations reveal a variety of intercage interactions in these materials, largely governed by pi-pi stacking. Density functional theory for a subset of these cages was used to confirm that the nature of the increased stability of aryl-functionalized cages is a result of inter-cage ligand interactions.

Porous molecular adsorbents, which include both all-organic[1] and metal-organic materials,[2] may have considerable advantages over extended, three-dimensional solids. Their molecular nature endows them with inherent solubility in a wide range of solvents.[3] From a synthesis standpoint, this allows for significantly more control as molecular level design strategies can be employed for the tailored installation of functional groups.[4] The lack of extended connectivity in porous molecules, however, typically results in lower surface areas and thermal stabilities as compared to their three-dimensional counterparts.[5,6] For many of these molecules, cage surface functionalization can be used to tune these properties.[7] This has been exhaustively leveraged in porous organic cages (POCs).[8] In terms of metal-organic molecular materials,[9,1011] ligand functionalization strategies have been used to tune solubility,[12] control phase,[13] and endow the materials with switchable post-synthetic reactivity.[14] In the well-known M_{24}(bdc)$_{24}$ (M = Cr, Ni, Cu, Mo, Ru, Rh; bdc^{2-} = isophthalic acid) cages,[4,9,15,16,17,18] functionalization of the 5-position of the bridging ligand is a straightforward route to tune material properties.[19]

We have recently shown that a related class of paddlewheel-based coordination cages show tremendous utility for the high-pressure storage of natural gas.[20,21,22,23] These M_{12}(cdc)$_{12}$ (M = Cr, Cu, Mo; cdc^{2-} = carbazole-dicarboxylate) cages feature high surface areas and optimal cage size and geometry for efficient methane storage.[16,20,24,25,] The carbazole-dicarboxylic acid ligand does feature the advantage in that it is compatible with straightforward functionalization on the 9-position of the ligand.[26,27,28,29] This has previously been targeted as a means to control phase in carbazole-based coordination cages.[30] However, the previously reported functionalized materials featured low surface areas, likely a result of the lack of inter-cage interactions via their appended isopropyl functional groups. Both alkylation and coupling chemistry are useful in this regard as a large library of functionalized ligands can be prepared for the isolation of surface-functionalized octahedral cages. Herein, we report the design, synthesis, and characterization of a family of functionalized carbazole-dicarboxylate paddlewheel cages (Figure 1). We demonstrate that the presence of aryl groups on the 9-position of the ligand affords molecular adsorbents with high surface areas and, for a subset of these cages, significantly increased thermal stability.

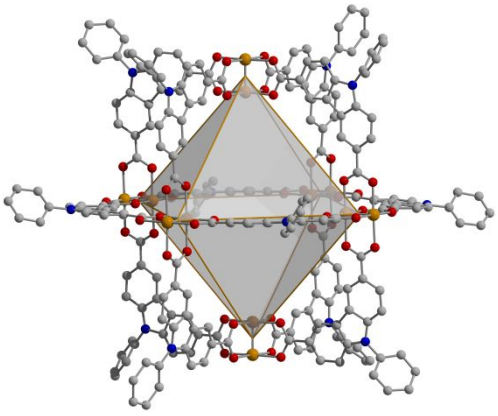

Fig. 1 Structure of an octahedral carbazole-based $M_{12}L_{12}$ coordination cage featuring 9-position functionalization. In this work the functional groups include phenyl, iPr-phenyl, biphenyl, carbazole, and ^{i}propyl. The orange, red, blue, and grey spheres represent molybdenum, oxygen, nitrogen, and carbon atoms, respectively. Hydrogen atoms have been omitted for clarity.

In addition to alkylation, the 9-position of carbazole is easily functionalized via Ullman coupling with aryl iodides to afford aryl-substituted ligands. These types of ligands are expected to endow coordination cages with strong and directional interactions in the solid state. We used this strategy of aryl substitution followed by

[a] Department of Chemistry and Biochemistry, University of Delaware, Newark, Delaware 19716, United States. E-mail: edb@udel.edu
[b] Center for Neutron Science, Department of Chemical and Biomolecular Engineering, University of Delaware, Newark, Delaware 19716, United States.
[c] Catalysis Center for Energy Innovation (CCEI) University of Delaware, Newark, Delaware, 19716, USA

† Electronic Supplementary Information (ESI) available: adsorption isotherms, crystallographic information, spectroscopic data. See DOI: 10.1039/x0xx00000x

acylation and oxidation to prepare a family of functionalized ligands (Figure 2). Copper (I) catalysed Ullman coupling of 9H-carbazole with 1-Iodo-4-isopropylbenzene or 4-Iodo-1,1'-biphenyl yielded 9-(4'-^{i}Prphenyl)-carbazole and 9-biphenyl-carbazole, respectively. Friedel-Crafts acylation reactions were then performed on these aryl-substituted carbazole units to obtain 3,6-diacetyl-9-(4'-^{i}Prphenyl)-carbazole and 3,6-diacetyl-9-biphenyl-carbazole. Commercially available 9-phenyl-carbazole and 9-(4'-bromophenyl)-carbazole were also subjected to Friedel-Crafts acylation reactions to yield 3,6-diacetyl-9-phenyl-carbazole and 3,6-diacetyl-9-(4'-bromophenyl)-carbazole, respectively. The aforementioned diacetyl derivatives were then oxidized to dicarboxylates with sodium hypobromite followed by acidification to afford the corresponding diacids. Esterification of the 9-(4'-bromophenyl)-carbazole-3,6-dicarboxylic acid with methyl iodide yields dimethyl 9-(4'-bromophenyl)-carbazole-3,6-dicarboxylate. Ullman coupling of this moiety with base 9H-carbazole yields dimethyl 9-(4'-carbazolylphenyl)-carbazole-3,6-dicarboxylate which is easily deprotected in base and acidified to afford the diacid.

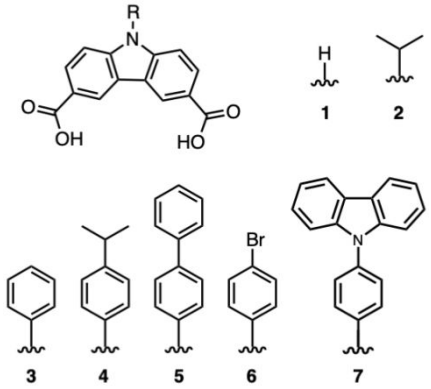

Fig. 2 Ligands used to prepare the octahedral coordination cages reported here. Where 1-7 represent 9H, 9-^{i}Pr, 9-phenyl, 9-^{i}Prphenyl, 9-biphenyl, 9-Br-phenyl and 9-carbazolyl-phenyl functionalization, respectively.

In order to obtain diffraction-quality single crystals of cages based on these ligands, we screened a variety of reaction conditions for Cr^{2+}, Cu^{2+}, and Mo^{2+} starting materials. Although copper(II) acetate has been previously used to afford cuboctahedral copper cages, reaction of this salt with the ligands reported here routinely gave amorphous powder that rapidly formed upon reagent mixing. This rapid product isolation is likely a result of the fast formation kinetics of cages when using a preformed paddlewheel unit as the reagent. Ultimately the reaction of copper nitrate with organic ligands in DMA at elevated temperature (100 °C) afforded crystalline product in high yield. However, the addition of pyridine or DMSO were required to obtain diffraction-quality single crystals for H_2bromophenyl-cdc and H_2carbazolyl-phenyl-cdc, respectively. Despite our best efforts, we were unable to obtain crystalline copper cages with the other ligands reported here.

In contrast to the synthesis of copper cages, where $Cu_2(OAc)_4$ gave amorphous products, utilization of the preformed paddlewheel unit was necessary for Cr^{2+} and Mo^{2+}. Although we screened reactions in a variety of polar organic solvents, including DMF, DMA, DEF, DMPU, and NMP, crystalline products were most reliably obtained from reaction in DMF or DMPU. The synthetic conditions to afford Cr_{12}(phenyl-cdc)$_{12}$, Cr_{12}(Br-phenyl-cdc)$_{12}$, Mo_{12}(phenyl-cdc)$_{12}$, Mo_{12}(Br-phenyl-cdc)$_{12}$, Mo_{12}(^{i}Pr-phenyl-cdc)$_{12}$, and Mo_{12}(biphenyl-cdc)$_{12}$ were rather dissimilar with syntheses requiring a range of synthetic protocols. These ranged from more typical solvothermal reactions analogous to MOF syntheses where crystalline product is obtained upon heating, to room temperature mixing of pre-heated solutions or diffusion/layering of a cosolvent on a pre-heated reaction mixture, akin to typical supramolecular syntheses. In terms of the aforementioned Cr^{2+} and Mo^{2+} cages, diffraction-quality single crystals were obtained for every material except Cr_{12}(phenyl-cdc)$_{12}$ and Mo_{12}(Br-phenyl-cdc)$_{12}$.

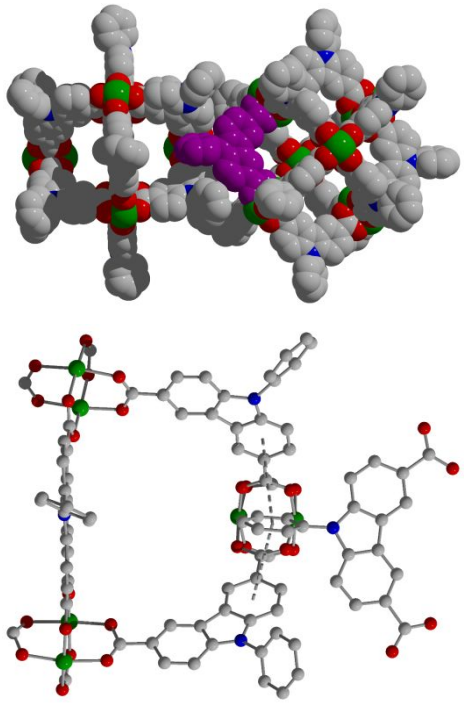

Fig. 3 Structure of Cu_{12}(phenyl-cdc)$_{12}$. This cage displays phenyl-carbazole interactions in the solid state which leads to an increased thermal stability as compared to Cu_{12}(cdc)$_{12}$. Green, grey, red, and blue spheres represent copper, carbon, oxygen, and nitrogen atoms, respectively. Hydrogen atoms and solvent molecules have been omitted.

Single-crystal X-ray diffraction confirms that these materials adopt the expected octahedral cage geometry featuring six di-metal paddlewheel units linked to 12 dicarboxylate ligands and an internal cage diameter (M-M distance) of 14-15 Å. The internal diameter of the cages varies by metal with the Cu-cages being the smallest at ~ 14 Å, followed by the Cr-cage at ~ 14.4 Å and the Mo-cages at ~ 15 Å. The packing diagrams of the Cu_{12}(phenyl-cdc)$_{12}$, Mo_{12}(phenyl-cdc)$_{12}$ and Mo_{12}(biphenyl-cdc)$_{12}$ cages indicate phenyl-phenyl interactions in the corner of the triangular pore in the solid state (as shown in Figure 3) which decrease the distance between cages. Cages with this type of inter-cage interaction typically have cage-to-cage distances (measured between the centre of adjacent cages) of ~ 24 Å. Mo_{12}(^{i}Pr-phenyl-cdc)$_{12}$ features a similar interaction with the isopropyl group on one cage sitting in the corner of the triangular pore of an adjacent cage. This interaction is less favourable than the phenyl-phenyl interaction with cage-to-cage distances of 26.4 Å. Cr_{12}(Br-phenyl-cdc)$_{12}$ features a similar phenyl-phenyl interaction in addition to bromo-phenyl interactions between the bromine group on one cage and a carbazole moiety on an

adjacent cage. This results in cage-to-cage distances of 23.1 Å (phenyl-phenyl) and 25.2 Å (bromo-phenyl). Cu_{12}(carbazolyl-phenyl-cdc)$_{12}$ also displays a favourable phenyl-phenyl interaction between the carbazole functional group and the corner of the triangular pore of an adjacent cage. This complex also displays π-π stacking of the phenyl spacer between the two carbazole moieties on adjacent ligands. Both of these interactions decrease the cage-to-cage distance in this complex to ~ 24 Å.

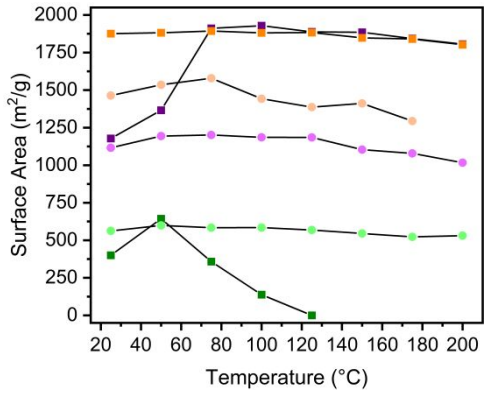

Fig. 4 Degas surveys for the copper (green), chromium (purple), and molybdenum (orange) cages where Langmuir surface areas are plotted as a function of activation temperature and dark squares or light circles represent 9H or 9-phenyl functionalization, respectively.

These inter-cage interactions in the solid-state have the potential to significantly impact the gas adsorption properties and thermal stability of these cages. The drawback to this interaction is that it will potentially limit the gas accessible surface area of these materials, which we have previously shown are highly dependent on a number of factors.[20] These can include space group into which the structure deposits, post-synthesis washing protocol, and activation conditions. As cages are molecular entities, they are often soluble in high-polarity solvents such as amides. Accordingly, direct solvent washes with more volatile organics after synthesis are required. For eight of the ten cages reported here direct room temperature methanol washes after cages synthesis were found to give the highest porosity samples, Cu_{12}(^{i}Pr-cdc)$_{12}$ and Cu_{12}(phenyl-cdc)$_{12}$ are compatible with DMA washes which are then followed by methanol washes.

For degas surveys, samples were placed under active vacuum at RT for 12 h or until the static off-gas rate ≤ 2 μbar/min. In order to increase the throughput of surface area measurements, partial isotherms were measured from which Langmuir surface areas could be calculated (Figure 4). Degas surveys were employed in 25 °C increments up to 200 °C. Upon determination of activation conditions, full isotherms from 0.001 – 0.9 P/P_0 were run on optimally activated materials to determine BET surface areas. As seen in Figure 4, the Cu-based aryl-functionalized-carbazole materials display a dramatic increase in their thermal stability as compared to their unfunctionalized counterpart. The surface area of Cu_{12}(cdc)$_{12}$ is optimized after an activation temperature of just 50 °C. The surface area of this cage markedly decreases at activation temperatures of 75 °C and 100 °C becoming non-porous at activation above 100 °C. The least thermally stable aryl-functionalized cage, Cu_{12}(carbazolyl-phenyl-cdc)$_{12}$, is optimally activated at 75 °C and displays decreases of less than 10 % of its optimal surface area through activation at 125 °C. The remaining materials reported herein display decreases of less than 20 % of their optimal surface area up to activation at 200 °C. The Cr- and Mo-based aryl-functionalized materials exhibit expected decreases in surface area as compared to unfunctionalized analogues due to pore and pore window blockage by the functional groups. However, for Cu-based cages the aryl-functionalized materials display very similar surface areas to Cu_{12}(cdc)$_{12}$ which is notably lower than expected based on the values displayed by Cr_{12}(cdc)$_{12}$ and Mo_{12}(cdc)$_{12}$. Optimized BET surface areas for these cages are listed in Table 1.

Table 1. BET surface areas (m²/g) of functionalized cages, M_{12}(R-cdc)$_{12}$.

R–goup	M = Cr	M = Cu	M = Mo
H[23]	1235	657	1108
^{i}Pr	–	205	–
Phenyl	846	313	909
Br-phenyl	421	373	859
Carbazolylphenyl	–	515	–
Biphenyl	–	–	716
^{i}Pr-phenyl	–	–	849

In order to assess the substitution effect on the thermal stability of the cages, we performed density-functional theory (DFT) calculations for truncated model structures of Mo_{12}(X-cdc)$_{12}$, where X (-Ph or -^{i}propyl) is the substituent at the 9-position of the carbazole dicarboxylate ligand. The calculations were performed at the M06-L/6-31G(d,p) theory level for all the atoms except for Mo,[31] which was modeled at the M06-L/LANL2DZ level. The spin state of the Mo-Mo dimer unit is found to be a singlet and a quadruple bond between Mo-Mo (d_{Mo-Mo}=2.12Å) was confirmed by NBO analysis. All the binding energies reported herein are BSSE corrected. All the calculations were performed with Gaussian 09.[32] The phenyl-substituted ligands exhibit considerable π-π stacking interactions, with π-π distance of 3.71 Å. The π-π interaction is mostly responsible for the significant binding energy of 14.5 kcal/mol between the two fragments shown in Figure 2. On the other hand, the iso-propyl-substituted ligands interact significantly less and the binding energy between them is only 3.1 kcal/mol. The stronger attractive interaction between the phenyl-substituted ligands is aligned with the experimentally observed greater thermal stability of the corresponding cages which we have confirmed via variable temperature powder X-ray diffraction (Figure S64). Here, Cu_{12}(phenyl-cdc)$_{12}$ essentially exhibits no decrease in crystallinity upon activation temperatures up to 225 °C whereas Cu_{12}(cdc)$_{12}$ is amorphous and nonporous at just 100 °C

The results shown here demonstrate that facile cross-coupling reactions can be used to afford aryl-functionalized carbazole ligands for construction of functionalized $M_{12}L_{12}$ coordination cages. The resulting chromium(II), copper(II) and molybdenum(II) cages represent the first examples of aryl-functionalized carbazole cages and display tuneable properties based on the nature of the carbazole substituent. Aryl-aryl

interactions are prevalent in the solid-state structures of these materials, and particularly in the case of Cu_{12}(R-phenyl-cdc)$_{12}$ result in surface areas, thermal stability, and crystallinity that is significantly higher than those displayed by the unfunctionalized cage. It is our expectation that these approaches can be leveraged for the continued development of novel porous coordination cages with tailorable bulk properties.

This manuscript was prepared under cooperative agreement #70NANB17H302 from NIST, U.S. Department of Commerce. This work utilized facilities supported in part by the National Science Foundation under Agreement No. DMR-0944772. This material is based upon work supported as part of the Catalysis Center for Energy Innovation, an Energy Frontier Research Center funded by the U.S. Department of Energy, Office of Science, Office of Basic Energy Sciences under Award Number DE-SC0001004. This work also used resources of the Advanced Photon Source, a U.S. Department of Energy (DOE) Office of Science User Facility operated for the DOE Office of Science by Argonne National Laboratory under Contract No. DE-AC02-06CH11357. We also thank the Delaware Space Grant College and Fellowship Program, NASA Grant NNX15AI19H, for fellowship support of C.A.R.

Conflicts of interest

There are no conflicts to declare.

References

1 T. Tozawa, J. T. A. Jones, S. I. Swamy, S. Jiang, D. J. Adams, S. Shakespeare, R. Clowes, D. Bradshaw, T. Hasell, S. Y. Chong, C. Tang, S. Thompson, J. Parker, A. Trewin, J. Bacsa, A. M. Z. Slawin, A. Steiner and A. I. Cooper, *Nat. Mater.*, 2009, **8**, 973-978.

2 D. J. Tranchemontagne, Z. Ni, M. O'Keeffe and O. M. Yaghi, *Angew. Chem. Int. Ed.*, 2008, **47**, 5136-5147.

3 E. V. Preez, K. J. Balkus Jr., J. P. Ferraris and I. H. Musselman, *J. Membr. Sci.*, 2014, **463**, 82-93.

4 J. Park, Z. Perry, Y.-P. Chen, J. Bae and H.-C. Zhou, *ACS Appl. Mater Interfaces*, 2017, **9**, 28064-28068.

5 G. R. Lorzing, E. J. Gosselin, B. S. Lindner, R. Bhattacharjee, G. P. A. Yap, S. Caratzoulas and E. D. Bloch, *Chem. Commun.*, 2019, **55**, 9527-9530.

6 G. E. Decker, G. R. Lorzing, M. M. Deegan and E. D. Bloch, *J. Mater. Chem. A*, 2020, **8**, 4217-4229.

7 S. Mollick, S. Fajal, S. Mukherjee and S. K. Ghosh, *Chem. Asian J.*, 2019, **14**, 3096-3108.

8 S. Jiang, J. T. A. Jones, T. Hasell, C. E. Blythe, D. J. Adams, A. Trewin and A. I. Cooper, *Nature Comm.*, 2011, **2**, 207-212.

9 M. Eddaoudi, J. Kim, J. B. Wachter, H. K. Chae, M. O'Keeffe and O. M. Yaghi, *J. Am. Chem. Soc.*, 2001, **123**, 4368-4369.

10 G. J. McManus, Z. Wang and M. J. Zaworotko, *Cryst. Growth Des.*, 2004, **4**, 11-13.

11 S. R.Seidel and P. J. Stang, *Acc. Chem. Res.*, 2002, **35**, 972-983.

12 W. Lu, D. Yuan, A. Yakovenko and H.-C. Zhou, *Chem. Commun.*, 2011, **47**, 4968-4970.

13 O. Barreda, G. Bannwart, G. P. A. Yap and E. D. Bloch, *ACS Appl. Mater Interfaces*, 2018, **10**, 11420-11424.

14 J. Park, L.-B. Sun, Y.-P. Chen, Z. Perry and H.-C. Zhou, *Angew. Chem. Int. Ed.*, 2014, **53**, 5842-5846.

15 E. J. Gosselin, C. A. Rowland, K. P. Balto, G. P. A. Yap and E. D. Bloch, *Inorg. Chem.*, 2018, **19**, 11847-11850.

16 J.-R. Li, A. A. Yakovenko, W. Lu, D. J. Timmons, W. Zhuang, D. Yuan and H.-C. Zhou, *J. Am. Chem. Soc.*, 2010, **132**, 17599-17610.

17 M. D. Young, Q. Zhang and H.-C. Zhou, *Inorg. Chim. Acta*, 2015, **424**, 216-220.

18 S. Furukawa, N. Horike, M. Kondo, Y. Hijikata, A. Carne-Sanchez, P. Larpent, N. Louvain, S. Diring, H. Sato, R. Matsuda, R. Kawano and S. Kitagawa, *Inorg. Chem.*, 2016, **55**, 10843-10846.

19 G. R. Lorzing, E. J. Gosselin, B. A. Trump, A. H. P. York, A. Sturluson, C. A. Rowland, G. P. A. Yap, C. M. Brown, C. M. Simon and E. D. Bloch, *J. Am. Chem. Soc.*, 2019, **141**, 12128-12138.

20 S. Krause, J. D. Evans, V. Bon, I. Senkovska, S. Ehrling, U. Stoeck, P. G. Yot, P. Iacomi, P. Llewellyn, G. Maurin, F.-X. Coudert and S. Kaskel, *J. Phys. Chem. C*, 2018, **122**, 19171-19179.

21 U. Stoeck, I. Senkovska, V. Bon, S. Krause and S. Kaskel, *Chem. Commun.*, 2015, **51**, 1046-1049.

22 S. Krause, V. Bon, I. Senkovska, U. Stoeck, D. Wallacher, D. M. Tobbens, S. Zander, R. S. Pillai, G. Maurin, F.-C. Coudert and S. Kaskel, *Nature*, 2016, **532**, 348-352.

23 C. A. Rowland, G. R. Lorzing, E. J. Gosselin, B. A. Trump, G. P. A. Yap, C. M. Brown and E. D. Bloch, *J. Am. Chem. Soc.*, 2018, **140**, 11153-11157.

24 A. Lopez-Olvera, E. Sanchez-Gonzalez, A. Campos-Reales-Pineda, A. Aguilar-Granda, I. A. Ibarra and B. Rodriguez-Molina, *Inorg. Chem. Front.*, 2017, **4**, 56.

25 J.-R. Li, D. J. Timmons and H.-C. Zhou, *J. Am. Chem. Soc.*, 2009, **131**, 6368-6369.

26 C. Huang, Y. Zhang, H. Yang, D. Wang, L. Mi, Z. Shao, M. Liu and H. Hou, *Cryst. Growth Des.*, 2018, **18**, 5674-5681.

27 V. Guillerm, L. J. Weselinski, Y. Belmabkhout, A. J. Cairns, V. D'Elia, L. Wojtas, K. Adil and M. Eddaoudi, *Nat. Chem.*, 2014, **6,** 673-680.

28 X. Jiang, Y. Liu, P. Wu, L. Wang, Q. Wang, G. Zhu, X.-L. Li and J. Wang, *RSC Adv.*, 2014, **4**, 47357-47360.

29 P. Wu, M. Jiang, Y. Li, Y. Liu, J. Wang, *J. Mater. Chem. A*, 2017, **5**, 7833-7838.

30 E. J. Gosselin, C. A. Rowland, K. P. Balto, G. P. A. Yap and E. D. Bloch, *Inorg. Chem.*, 2018, **19**, 11847-11850.

31 Y. Zhao and D.G. Truhlar, *Theor. Chem. Acc.* **2008**, *120*, 215.

32 Gaussian 09, Revision D.01, M. J. Frisch, G. W. Trucks, H. B. Schlegel, G. E. Scuseria, M. A. Robb, J. R. Cheeseman, G. Scalmani, V. Barone, B. Mennucci, G. A. Petersson, H. Nakatsuji, M. Caricato, X. Li, H. P. Hratchian, A. F. Izmaylov, J. Bloino, G. Zheng, J. L. Sonnenberg, M. Hada, M. Ehara, K. Toyota, R. Fukuda, J. Hasegawa, M. Ishida, T. Nakajima, Y. Honda, O. Kitao, H. Nakai, T. Vreven, J. A. Montgomery, Jr., J. E. Peralta, F. Ogliaro, M. Bearpark, J. J. Heyd, E. Brothers, K. N. Kudin, V. N. Staroverov, T. Keith, R. Kobayashi, J. Normand, K. Raghavachari, A. Rendell, J. C. Burant, S. S. Iyengar, J. Tomasi, M. Cossi, N. Rega, J. M. Millam, M. Klene, J. E. Knox, J. B. Cross, V. Bakken, C. Adamo, J. Jaramillo, R. Gomperts, R. E. Stratmann, O. Yazyev, A. J. Austin, R. Cammi, C. Pomelli, J. W. Ochterski, R. L. Martin, K. Morokuma, V. G. Zakrzewski, G. A. Voth, P. Salvador, J. J. Dannenberg, S. Dapprich, A. D. Daniels, O. Farkas, J. B. Foresman, J. V. Ortiz, J. Cioslowski, and D. J. Fox, Gaussian, Inc., Wallingford CT, 2013.